

# OPTIMUM DRIVE CIRCUITS FOR POWER TRANSISTOR SWITCHING

## INTRODUCTION

In this note the physical phenomenon is examined which, in general, determines the switching times of a transistor. Particular attention is devoted to the fall time of the collector current, which causes the amount of the energy lost during the turn-off phase of the device, and can cause its thermal runaway.

This is the most common failure occurring to the BU806 when used as the final stage in monochrome CRT deflection circuits. Some results are reported for this device in order to define the optimum dimensioning of its driving circuitry.

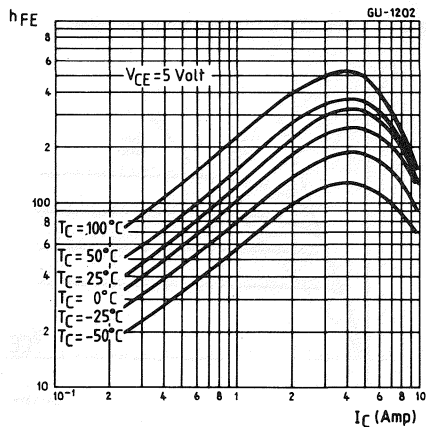
## TURN-ON PHASE

The conduction phase of the transistor depends on the value of the direct base current, which has to be adequate to ensure the device saturation for the relevant operating collector currents.

The turn-on phase is regulated by the positive slope of the base current, which must be as high as possible in order to minimize the losses during this phase.

The graphs of fig. 1 show the behaviour of the  $h_{FE}$  versus several temperature and collector current values for a BU806 device which has been chosen in the lowest range of the  $h_{FE}$  distribution. It shows that a forced  $h_{FE}$  of 100 is sufficient to ensure that the BU806 is saturated in the range of collector currents between 1 and 9 amp and in the range of temperatures between  $0^{\circ}\text{C}$  and  $T_{J\text{MAX}}$ .

Fig. 1 -  $h_{FE}$  parameter vs. temperature and collector current

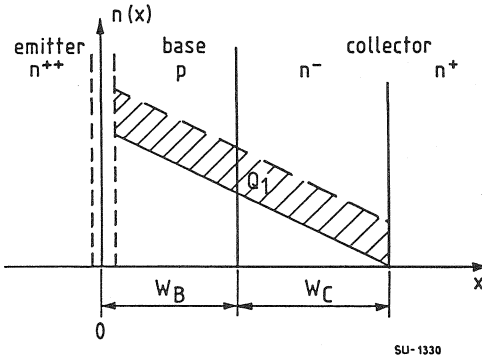


## TURN-OFF PHASE

The turn-off of a transistor, which is in a saturated state, is performed by removing the electric charge from the base and from the portion of the collector which is invaded by the excess base charges.

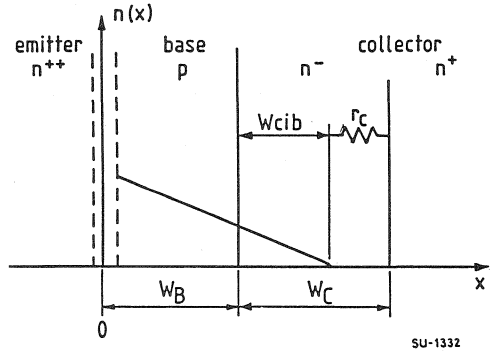
The dotted line of fig. 2 qualitatively shows the charge distribution of a transistor in the saturation phase.

Fig. 2 - Charge distribution of a saturated transistor



SU-1330

Fig. 4



SU-1332

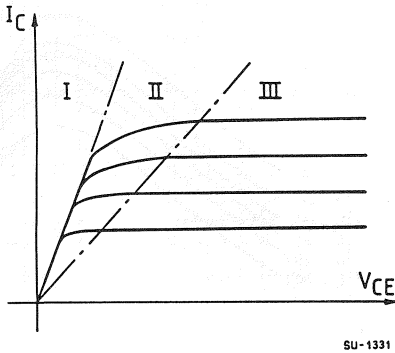
An inverse base current is imposed through the base to remove the electric charge

$$Q = \rho_0 W_b + W_{cib} n(x) dx \quad (1)$$

where  $W_b$  is the base width and  $W_{cib}$  is the part of the collector invaded by the base charge.

The extraction of  $Q_1$  charge of fig. 2 does not cause a variation of the collector current or of the collector emitter voltage. In the output characteristics of fig. 3 the device is in the region I.

Fig. 3 - Common emitter characteristics



SU-1331

Continuing to extract further electric charge through the base, the charge distribution becomes as shown in fig. 4: the collector current remains unchanged, while the collector emitter voltage rises because the series collector resistance  $r_C$  increases.

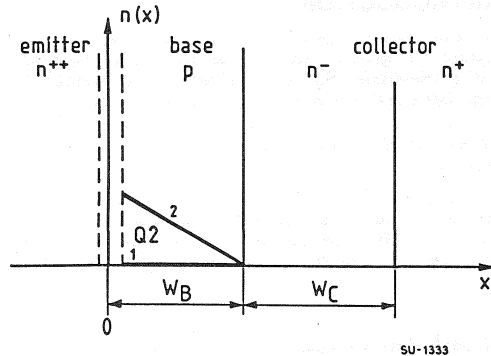
$$r_C = \rho_C \times (W_c - W_{cib}) / A_E \quad (2)$$

where  $\rho_C$  is the collector resistivity and  $A_E$  is the emitter area.

In the output characteristics of fig. 3 the  $V_{CE} - I_C$  locus is in the region II of quasi saturation. This situation persists while the collector charge is not completely evacuated (see fig. 5).

The time elapsed in order to pass from the charge distribution of fig. 2 (dotted line) to the distribution of fig. 5 (line 2) is defined as storage time ( $t_s$ ).

Fig. 5 - Charge distribution after  $t_s$



SU-1333

Then the collector current goes down until the electric charges in the base are removed, while the collector emitter voltage reaches its maximum value. The time elapsed to pass from distribution 2 to distribution 1 of fig. 5 is defined as the collector current fall time ( $t_f$ ).

The various phases described above are determined by the waveform of the base current. An extraction, which is too weak, increases either  $t_s$  or  $t_f$ , but an extraction, which is too strong, decreases the  $t_s$  parameter but it can increase the  $t_f$  if the B-E junction becomes reverse biased before all the charge quantity  $Q_2$  of fig. 5 is evacuated. In such a situation the base charge is removed only by recombination and a long tail can be seen on the collector current (see fig. 6).

Fig. 6

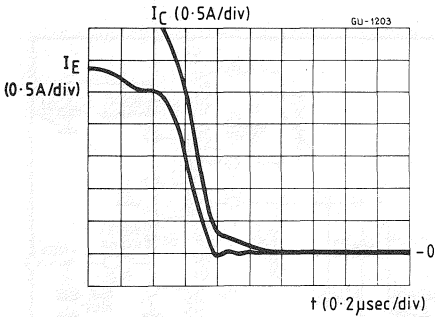
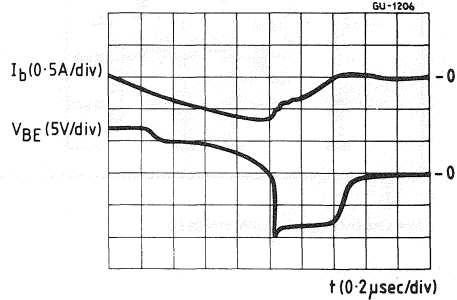
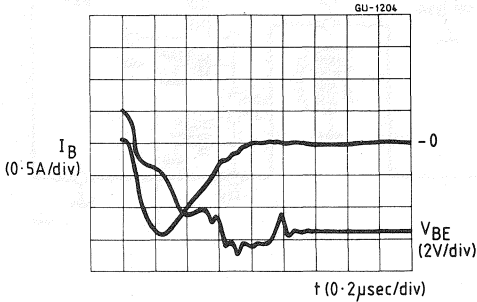
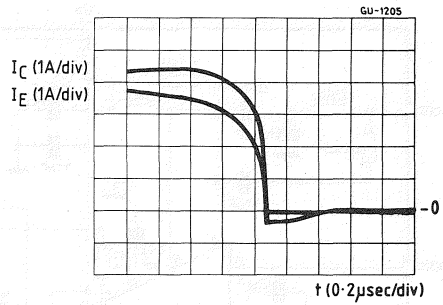
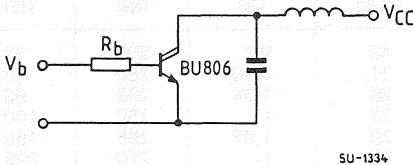


Fig. 9



The basic circuit used to verify this phenomenon is showing in fig. 7.

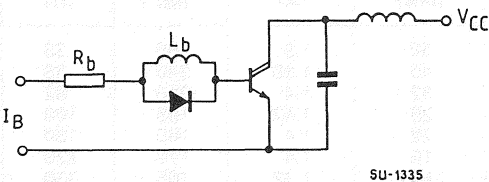
Fig. 7 - Basic test driving circuit



SU-1334

If an inductor is added in series with the base, as shown in fig. 8, a better collector current behaviour is noted during the turn-off (see fig. 9).

Fig. 8 - Basic driving test circuit with a base inductor



SU-1335

As displayed in fig. 9 the B-E junction goes into reverse breakdown, that is the remaining electric charges in the base are removed by achieving their evacuation with a negative emitter current.

Now it can be argued that the optimal operative condition is when the collector current and the emitter current go to zero simultaneously.

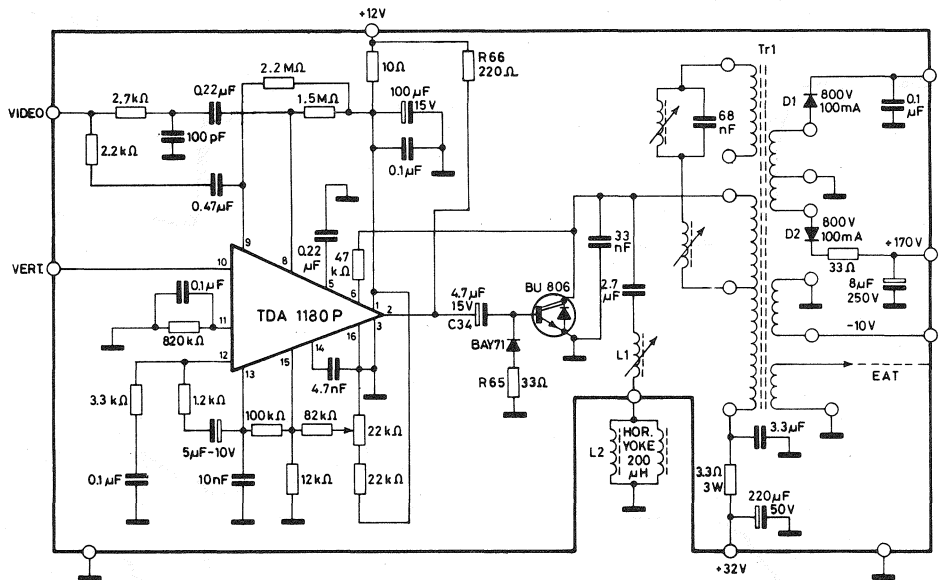
Hence the aim of the report will be to find the optimum solution for the BU806 device.

## BU806 DRIVING

In the application of the BU806 as the final stage of the horizontal deflection (see fig. 9) the most critical phase is in the fall of the collector current, which causes the amount of the power dissipated in the turn-off and can give rise to the thermal runaway of the device.

Many tests were performed by changing components of the driving circuitry R66, C34 and R65 in the schematic diagram of fig. 10. The relative waveforms of  $I_C$  and  $V_{CE}$  are shown in fig. 11 and 12.

Fig. 10 - Basic schematic diagram of the monitor



L1 = Linearity inductance RL 33 INELCO

S-2887/3

Fig. 11

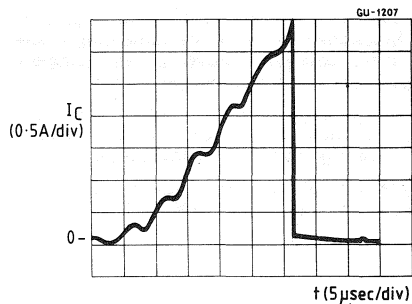
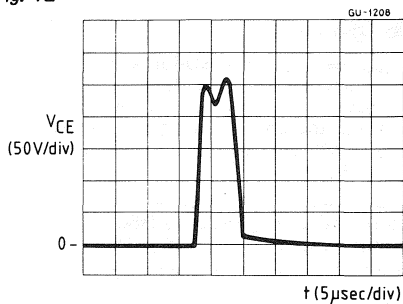


Fig. 12



The results are reported in the tables 1 to 9.

Table 1 - C34 = 3.3µF, R66 = 68Ω, T<sub>C</sub> = 35°C

I <sub>B1</sub> (mA)	I <sub>B2</sub> (A)	t <sub>f</sub> (ns)	R65 (Ω)
42	0.9	300	33
31	0.96	260	68
28	1.04	255	82
23	1	250	100
20	1.02	235	150
15	1	210	220
12	0.96	210	330

Table 2 - C34 = 4.7µF, R66 = 68Ω, T<sub>C</sub> = 35°C

I <sub>B1</sub> (mA)	I <sub>B2</sub> (A)	t <sub>f</sub> (ns)	R65 (Ω)
50	1.3	285	33
40	1.36	240	68
32	1.4	210	82
28	1.42	195	100
22	1.4	180	150
16	1.4	170	220
14	1.32	165	330

**Table 3** - C34 = 6.8 $\mu$ F, R66 = 68 $\Omega$ , T<sub>C</sub> = 35 $^{\circ}$ C

I <sub>B1</sub> (mA)	I <sub>B2</sub> (A)	t <sub>f</sub> (ns)	R65 ( $\Omega$ )
50	1.3	270	33
36	1.36	215	68
30	1.4	190	82
27	1.4	190	100
22	1.4	165	150
16	1.36	160	220
13	1.28	150	330

**Table 7** - C34 = 3.3 $\mu$ F, R66 = 150 $\Omega$ , T<sub>C</sub> = 35 $^{\circ}$ C

I <sub>B1</sub> (mA)	I <sub>B2</sub> (A)	t <sub>f</sub> (ns)	R65 ( $\Omega$ )
33	0.65	460	33
27	0.69	400	68
23	0.77	340	82
22	0.8	320	100
18	0.83	280	150
15	0.87	250	220
14	0.89	240	330

**Table 4** - C34 = 3.3 $\mu$ F, R66 = 82 $\Omega$ , T<sub>C</sub> = 35 $^{\circ}$ C

I <sub>B1</sub> (mA)	I <sub>B2</sub> (A)	t <sub>f</sub> (ns)	R65 ( $\Omega$ )
42	0.86	320	33
31	0.92	285	68
28	0.96	280	82
26	0.96	240	100
20	0.96	210	150
15	1	205	220
14	0.96	180	330

**Table 8** - C34 = 4.7 $\mu$ F, R66 = 150 $\Omega$ , T<sub>C</sub> = 35 $^{\circ}$ C

I <sub>B1</sub> (mA)	I <sub>B2</sub> (A)	t <sub>f</sub> (ns)	R65 ( $\Omega$ )
34	0.98	340	33
30	1	285	68
28	1.24	240	82
26	1.28	225	100
22	1.32	220	150
18	1.36	210	220
15	1.36	190	330

**Table 5** - C34 = 4.7 $\mu$ F, R66 = 82 $\Omega$ , T<sub>C</sub> = 35 $^{\circ}$ C

I <sub>B1</sub> (mA)	I <sub>B2</sub> (A)	t <sub>f</sub> (ns)	R65 ( $\Omega$ )
44	1.16	275	33
34	1.28	230	68
30	1.3	200	82
26	1.3	185	100
22	1.32	180	150
17	1.32	170	220
15	1.32	165	330

**Table 9** - C34 = 6.8 $\mu$ F, R66 = 150 $\Omega$ , T<sub>C</sub> = 35 $^{\circ}$ C

I <sub>B1</sub> (mA)	I <sub>B2</sub> (A)	t <sub>f</sub> (ns)	R65 ( $\Omega$ )
30	0.94	315	33
26	1.08	280	68
24	1.12	260	82
22	1.16	245	100
20	1.22	215	150
17	1.25	200	220
15	1.26	200	330

**Table 6** - C34 = 6.8 $\mu$ F, R66 = 82 $\Omega$ , T<sub>C</sub> = 35 $^{\circ}$ C

I <sub>B1</sub> (mA)	I <sub>B2</sub> (A)	t <sub>f</sub> (ns)	R65 ( $\Omega$ )
45	1.2	290	33
34	1.28	230	68
30	1.32	210	82
27	1.34	200	100
22	1.36	180	150
17	1.32	160	220
13	1.24	160	330

Based on these measurements the choice becomes:

- R66 = 68 $\Omega$
- C34 = 4.7 $\mu$ F
- R65 = 68 $\Omega$

which allows a low t<sub>f</sub> to be reached and assures the device saturation with a forced  $h_{FE}$  100.

These results were verified on other devices as the above analysis was performed on a typical piece. During this verification some devices were found which show a tail in the fall of the collector current (see fig. 13).

This is an undesirable condition because in this application the collector current crosses the V<sub>CE</sub>

path during the last part of its fall. Therefore this tail causes the greatest amount of the power dissipated in the device during turn-off.

Fig. 13

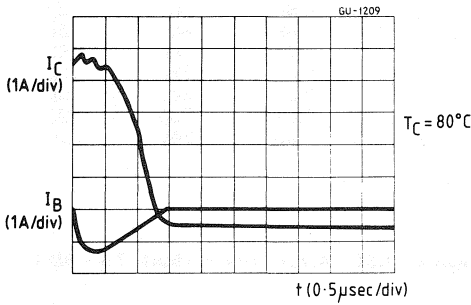


Fig. 14

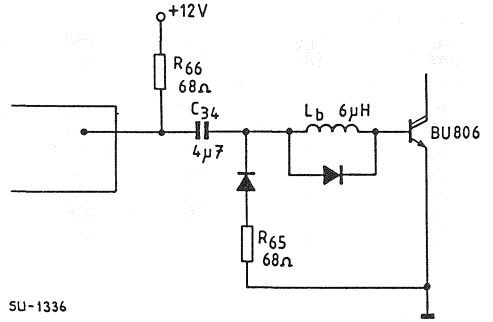
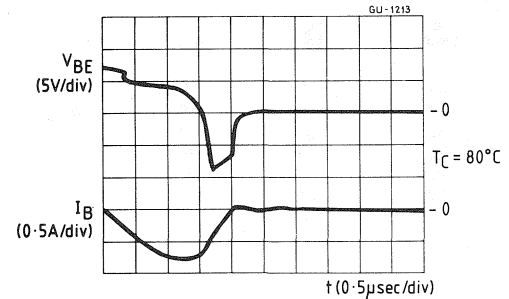
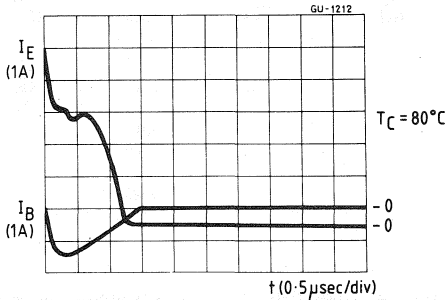
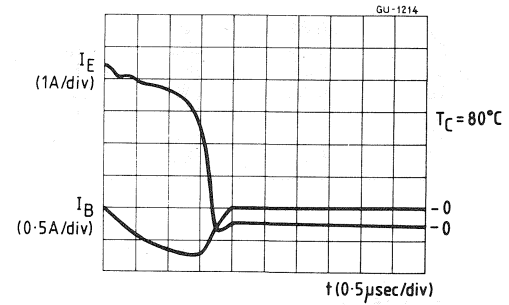
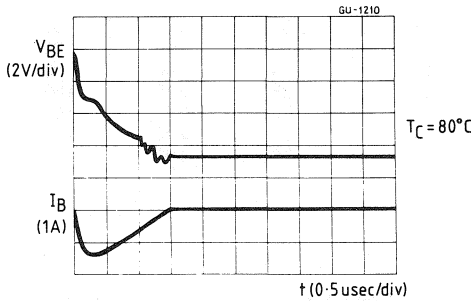


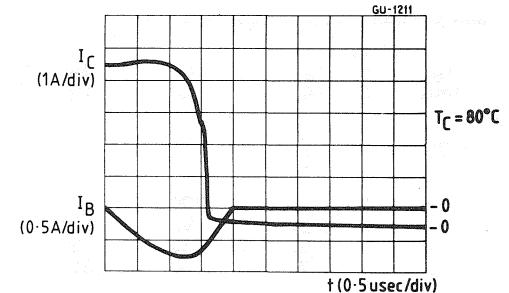
Fig. 15



A change was made in the driving circuitry as shown in fig. 14.

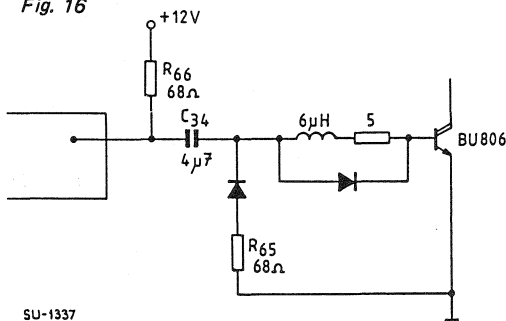
Comparing fig. 15 and fig. 13 it is to be noted that the maximum reverse base current is reduced to 800mA and is delayed by about 1µs. The effect of this delay on the base current peak toward the fall phase has been to decrease the value of  $t_f$ .

This is a satisfactory result but the tail in the collector current during turn-off is still present and the B-E junction goes into breakdown condition (see fig. 15).



An improvement in this situation has been achieved by changing the driving circuitry as shown in fig. 16.

Fig. 16



The result is that the reverse base current has a flatter shape and its maximum value is further reduced. Also the B-E junction is not driven into an avalanche condition and the collector and emitter currents become zero simultaneously, as shown in fig. 17.

Although the  $t_f$  has slightly increased, the energy dissipated in the turn-off phase is less than the previous driving circuit (see fig. 10 and fig. 14). Many other BU806 devices of several production lots were tested, obtaining good results with this driving circuitry.

Fig. 17

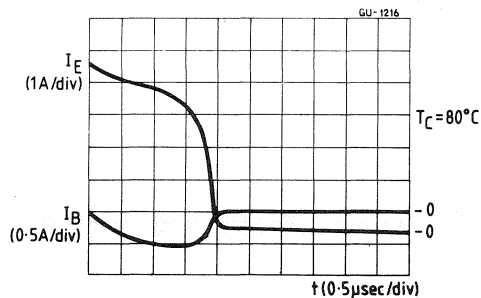
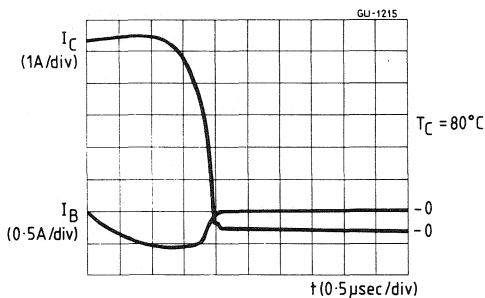


Fig. 17 - (continued)

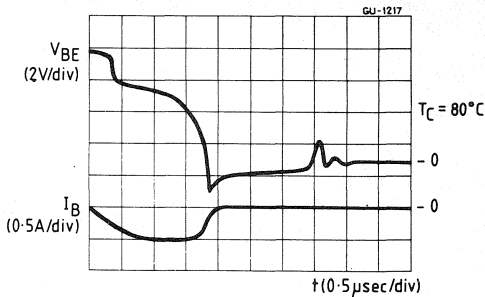


Fig. 18 -  $V_{CE} - I_C$  waveforms during the turn-off phase with the driving circuit of fig. 14.

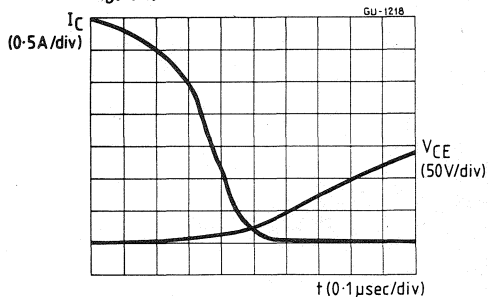
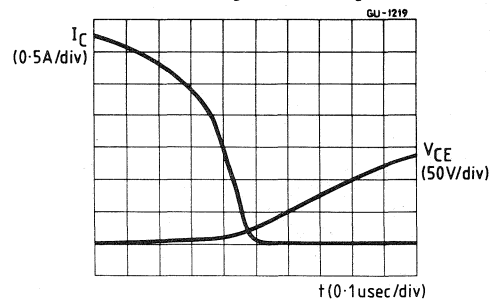


Fig. 19 -  $V_{CE} - I_C$  waveforms during turn-off with the driving circuit of fig. 16



## CONCLUSION

This report proposes a solution to the thermal runaway problem which may cause the most BU806 failures in the application as final stage of monochrome CRT horizontal deflection.

The component values of the driving circuitry of fig. 16, which are defined in this note, are typical of the monitor, in which the analysis has been performed (see fig. 10); they essentially depend on the collector current, which the device has to handle, and on the supply voltage of the driving circuitry.

However the philosophy used to reach these values can be employed for any other circuit structure as well as for other bipolar power transistors.